The First Case of Actinide Triple Helices: pH-Dependent Structural Evolution and Kinetics Controlled Transformation of Two Supramolecular Conformational Isomers

Shu-wen An, ‡ Lei Mei, ‡ Cong-zhi Wang, Chuan-qin Xia,* Zhi-fang Chai, and Wei-qun Shi*

Supporting Information

Table of contents

the single chain compound **1** with its intra-chain π-π stacking interactions.

Figure S9. Optimized structures of compounds **1** (a) and **2** (b) by the B3LYP method. White, green, blue, red, yellow, and pink spheres represent H, C, N, O, S, and U, respectively.

Figure S10. The main molecular orbitals (MOs) referring to the U-O and U-N bonding for compounds **1** and **2**.

Figure S11. Powder x-ray diffraction (PXRD) patterns demonstrating pH-dependent structural evolution of compounds **1** and **2**. From bottom to top: simulated PXRD of compound **1**; PXRD of solid product at pH=5.44; PXRD of solid product at pH=5.10; PXRD of solid product at pH=4.60; PXRD of solid product at pH=3.97; simulated PXRD of compound **2**.

Figure S12. PXRD results before and after the transformation of compound **2** to compound **1** with simulated PXRD patterns of compounds **1** and **2** for comparison: the trial of transformation for **2** in the presence of mother solution reveals the obvious change of PXRD patterns, giving characteristic peaks of compound **1**, whereas the attempt of direct transformation from a solid state of compound **2** in the absence of mother solution shows no change of PXRD patterns before and after the transformation.

Table S1. Selected bond distances (Å) related to uranyl centers and distances (Å) for hydrogen bonds and C-H•••π bonds observed in uranyl compounds **1** and **2**.

Table S2. Comparison of Selected Calculated and Experimental Bond Lengths (Å) of the U-O Bonds, and the May Bond Order (MBO) of the U-O Bonds for Compounds **1** and **2**.

Table S3. Percent Contribution of the U-O and U-N Bonding in Compounds **1** and **2**.

S1. General Methods

Caution! Suitable measures for precautions and protection should be taken, and all operations should follow the criteria while handling such substances although natural uranium was used in the experiment. All the reagents including 4, 4'-dicarboxybiphenyl sulfone (**H_2dbsf**) and 1,10-phenanthroline (**phen**) were obtained commercially and used as received.

Solid-state fluorescence spectra were measured on a Hitachi F-4600 fluorescence spectrophotometer. Powder XRD measurements were recorded on a Bruker D8 Advance diffractometer with Cu Kα radiation (λ=1.5406 Å) in the range 5-50° (step size: 0.02º). Thermogravimetric analysis (TGA) was performed on a TA Q500 analyzer over the temperature range of 30-800 °C in air atmosphere with a heating rate of 5 °C/min.

Synthesis of UO_2(dbsf)(phen) (1)

A mixture of $UO_2(NO_3)_2 \cdot 6H_2O$ (200 uL, 0.10 mmol), 4,4'-dicarboxybiphenyl sulfone（30.6 mg, 0.10 mmol）, 1,10-phenanthroline (18.0 mg, 0.10 mmol) and H_2O (2 ml) was placed in a Teflon-lined stainless steel vessel. After treating with NaOH, the mixture was sealed, kept at 180°C for 72 h and cooled to room temperature slowly. Yellow platelike crystals were washed with water and ethanol and dried in air.

Synthesis of [UO_2(dbsf)(phen)]·H_2O (2)

Compound **2** was obtained using the same procedure as that for **1** except that the pH of the mixture (3.97) was adjusted to 5.44. Yellow block crystals were washed with water and ethanol and dried in air.

pH-dependent structural evolution of compounds 1 and 2

Similar to the hydrothermal synthesis procedure of compounds **1** and **2**, different pH values (4.60 and 5.10) were adjusted to explore the pH-dependent structural evolution.

Crystal transformation from compound 2 to compound 1

The synthesized yellow block crystals of compound **2** were further incubated in the mother solution at 180 °C for 24 h, followed by fast cooling to room temperature within 2 h to obtain the yellow-green plate-like crystals.

In order to explore the transformation mechanism, a control experiment was conducted by incubating the crystals of compound 2 without any solution at 180 °C for 24 h, followed by fast cooling to room temperature within 2 h.

X-ray Single Structural Determination

X-ray diffraction data collection of compounds **1** and **2** performed with synchrotron radiation facility at BSRF (beamline 3W1A of Beijing Synchrotron Radiation Facility, λ = 0.71073 Å) using a MAR CCD detector. The crystal was mounted in nylon loops and cooled in a cold nitrogen-gas stream at 100 K. Data were indexed, integrated and scaled using DENZO and SCALEPACK from the HKL program suite (Otwinowski & Minor, 1997). The crystal structures were solved by means of direct methods and refined with full-matrix least squares on SHELXL-97.

Crystal data for **1**: $C_{26}H_{16}N_2O_8SU$, UO_2(dbsf)(phen), Mr = 754.50, Orthorhombic, $P2_12_12_1$, a = 8.4350(17) Å, b = 12.595(3) Å, c = 22.468(5) Å, V = 2387.0(8) $Å^3$, Z = 4, $\rho_{calcd.}$= 2.100 $g \cdot cm^{-3}$. The crystal structures were solved by means of direct methods and refined with full-matrix least squares on SHELXL-97 and converged to R_1 = 0.0367 and wR_2 = 0.0919, and GOF = 1.047 (Rint = 0.0412) for 4248 reflections [I > 2σ(I)].

Crystal data for **2**: $C_{26}H_{18}N_2O_9SU$, $[UO_2(dbsf)(phen)]\cdot H_2O$, Mr = 772.51, Monoclinic, $P2_1/c$, a =14.395(3) Å, b = 8.6750(17) Å, c = 20.368(4) Å, β= 95.16(3)°, V = 2533.2(9) $Å^3$, Z = 4, ρ_{calcd} = 2.026 $g \cdot cm^{-3}$, The crystal structures were solved by means of direct methods and refined with full-matrix least squares on SHELXL-97 and converged to R_1 = 0.0462 and wR_2 = 0. 1113, and GOF = 1.037. (Rint = 0.0307) for 4469 reflections [I > 2σ(I)].

Quantum chemistry calculation

For the model fragments of the uranyl complexes **1** and **2**, density functional theory (DFT) calculations were carried out by using the Gaussian 09 program package[1] with the B3LYP[2,3] hybrid functional. The quasi-relativistic effective core potentials (RECP) included 60 core electrons and the corresponding valence basis sets[4-6] were used for uranium, while the 6-31G(d) basis sets were adopted for light atoms (H, C, N, and O). The geometry optimization was performed without any symmetry constraints. At the same level of theory, harmonic vibrational frequency calculations have been carried out to verify the minima character of the optimized structures. Besides, the quantum theory of atoms in molecules (QTAIM)[7-10] analysis was performed by using Multiwfn 3.3.7 package.

References:

(1) Frisch, M. J.; Trucks, G. W.; Schlegel, H. B.; Scuseria, G. E.; Robb, M. A.; Cheeseman, J. R.; Montgomery, Jr., J. A.; Vreven, T.; Kudin, K. N.; Burant, J. C.; Millam, J. M.; Iyengar, S. S.;

Tomasi, J.; Barone, V.; Mennucci, B.; Cossi, M.; Scalmani, G.; Rega, N.; Petersson, G. A.; Nakatsuji, H.; Hada, M.; Ehara, M.; Toyota, K.; Fukuda, R.; Hasegawa, J.; Ishida, M.; Nakajima, T.; Honda, Y.; Kitao, O.; Nakai, H.; Klene, M.; Li, X.; Knox, J. E.; Hratchian, H. P.; Cross, J. B.; Bakken, V.; Adamo, C.; Jaramillo, J.; Gomperts, R.; Stratmann, R. E.; Yazyev, O.; Austin, A. J.; Cammi, R.; Pomelli, C.; Ochterski, J. W.; Ayala, P. Y.; Morokuma, K.; Voth, G. A.; Salvador, P.; Dannenberg, J. J.; Zakrzewski, V. G.; Dapprich, S.; Daniels, A. D.; Strain, M. C.; Farkas, O.; Malick, D. K.; Rabuck, A. D.; Raghavachari, K.; Foresman, J. B.; Ortiz, J. V.; Cui, Q.; Baboul, A. G.; Clifford, S.; Cioslowski, J.; Stefanov, B. B.; Liu, G.; Liashenko, A.; Piskorz, P.; Komaromi, I.; Martin, R. L.; Fox, D. J.; Keith, T.; Al-Laham, M. A.; Peng, C. Y.; Nanayakkara, A.; Challacombe, M.; Gill, P. M. W.; Johnson, B.; Chen, W.; Wong, M. W.; Gonzalez, C.; and Pople, J. A. *Gaussian 09 Revision A.02*; Gaussian, Inc.: Wallingford CT, 2009.

(2) Becke, A. D. *J. Chem. Phys.* 1993, *98*, 5648.

(3) Lee, C.; Yang, W.; Parr, R. G. *Phys. Rev. B* 1988, *37*, 785.

(4) Kuchle, W.; Dolg, M.; Stoll, H.; Preuss, H. *J. Chem. Phys.* 1994, *100*, 7535.

(5) Cao, X.; Dolg, M. *J. Molec. Struct.* (THEOCHEM) 2004, *673*, 203.

(6) Dolg, M.; Stoll, H.; Preuss, H. *J. Chem. Phys.* 1989, *90*, 1730.

(7) Bader, R. F. W., *Atoms in Molecules: A Quantum Theory*. Oxford University Press: Oxford, U.K., 1990.

(8) Bader, R. F. W., *J. Phys. Chem. A* 1998, *102*, 7314.

(9) Bader, R. F. W., *Chem. Rev.* 1991, *91*, 893.

(10) Lu, T.; Chen, F., *J. Comp. Chem.* 2012, *33*, 580.

S2. Typical figures and tables

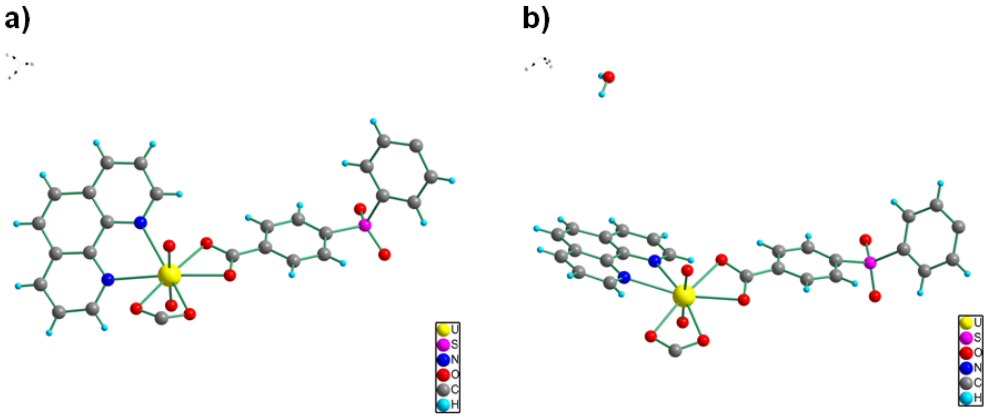

Figure S1. Coordination environments of uranyl center in compounds **1** (a) and **2** (b).

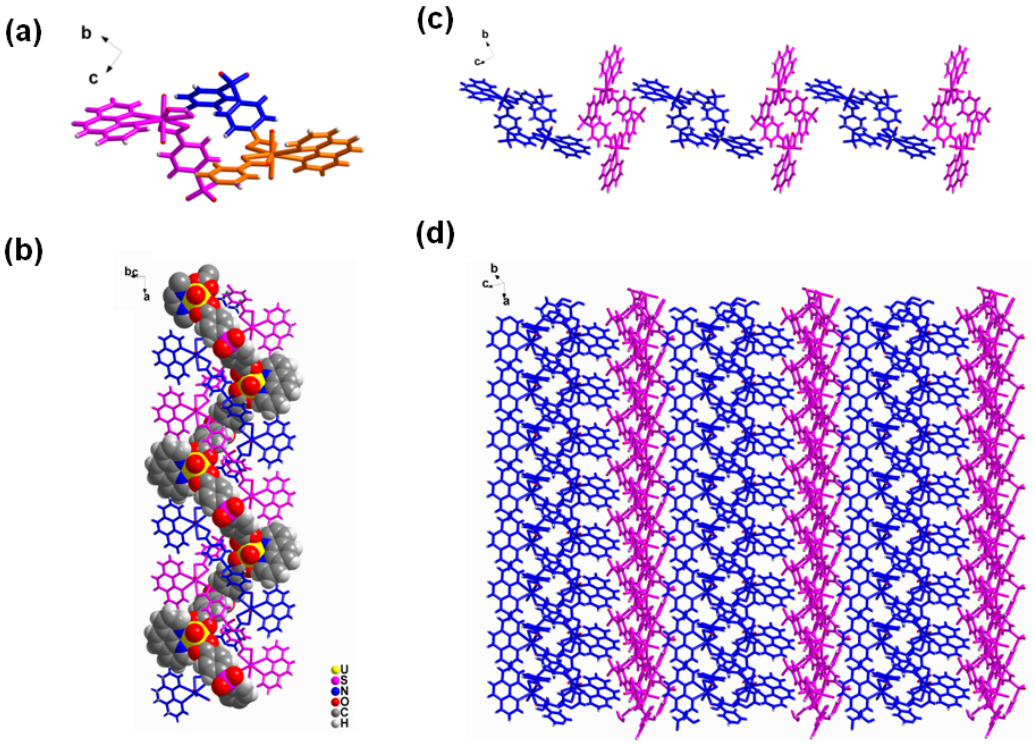

Figure S2. Side view of single chain triple-stranded helices of compound **1** from *a* axis (a) and *b* axis (b); close packing of compound **1** along *c* axis viewed from *a* axis (c) and *b* axis (d), which give separated single chain triple-stranded helices.

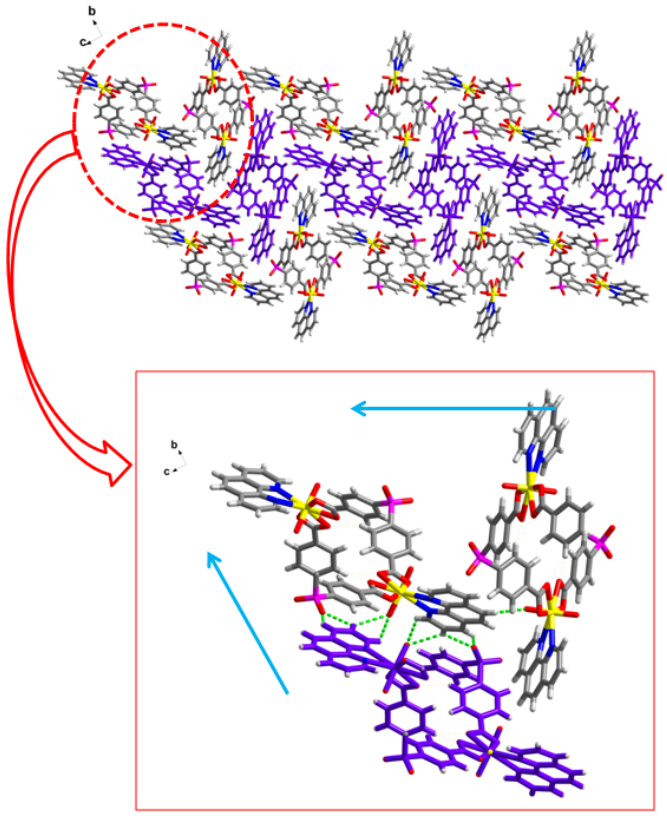

Figure S3. Close packing of compound **1** in three dimeonsions viewed from *a* axis (top) and weak hydrogen bonds connecting the sperated single chain triple-stranded helices (bottom): Along *b* axis, C(18)-H(18)•••O(8), 2.598(6) Å, C(17)-H(17)•••O(8), 2.712(6) Å, C(17)-H(17)•••O(5), 2.789(7) Å, C(16)-H(16)•••O(5), 2.775(6) Å; along *c* axis, C(27)-H(27)•••O(6), 2.538(7) Å.

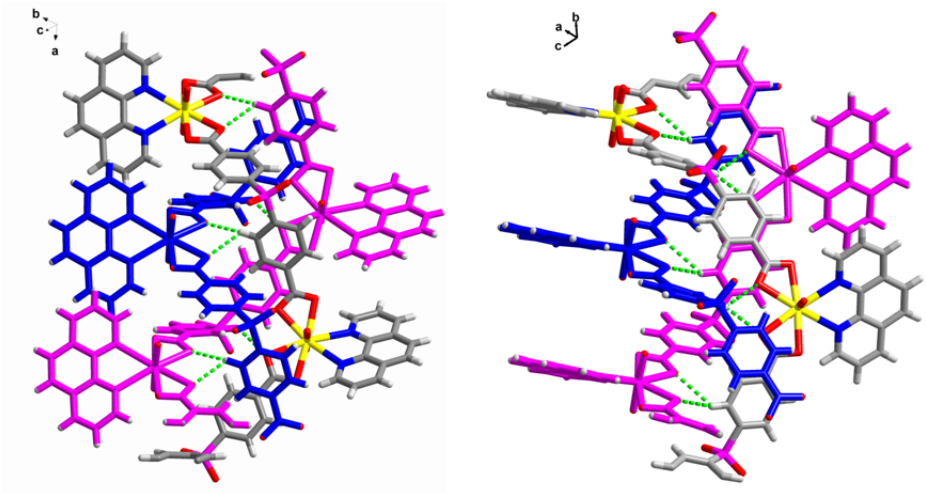

Figure S4. C-H•••O hydrogen bonds between different proximal strands in space contributing to the stabilization of uranyl triple-stranded helices for compound **1** (left, C(14)-H(14)•••O(2), 2.532(5) Å, C(14)-H(14)•••O(3), 2.511(6) Å) and compound **2** (right, C(11)-H(11)•••O(2), 2.716(4) Å, C(11)-H(11)•••O(3), 2.686(4) Å).

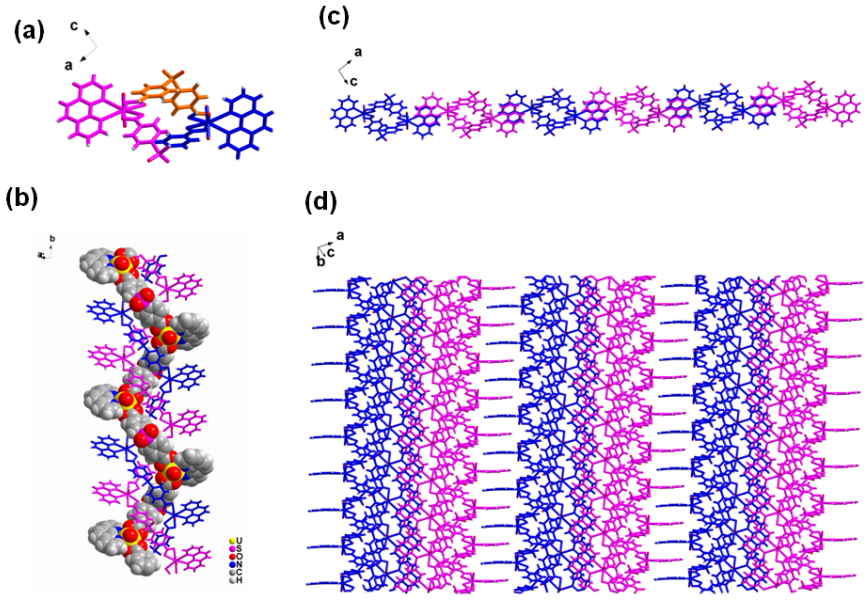

Figure S5. Side view of single chain triple-stranded helices of compound **2** from *b* axis (a) and *c* axis (b); close packing of compound **2** along *ac* plane viewed from *b* axix (c) and *c* axis (d), which give a 2D uranyl coordination network through inter-chain π-π interaction.

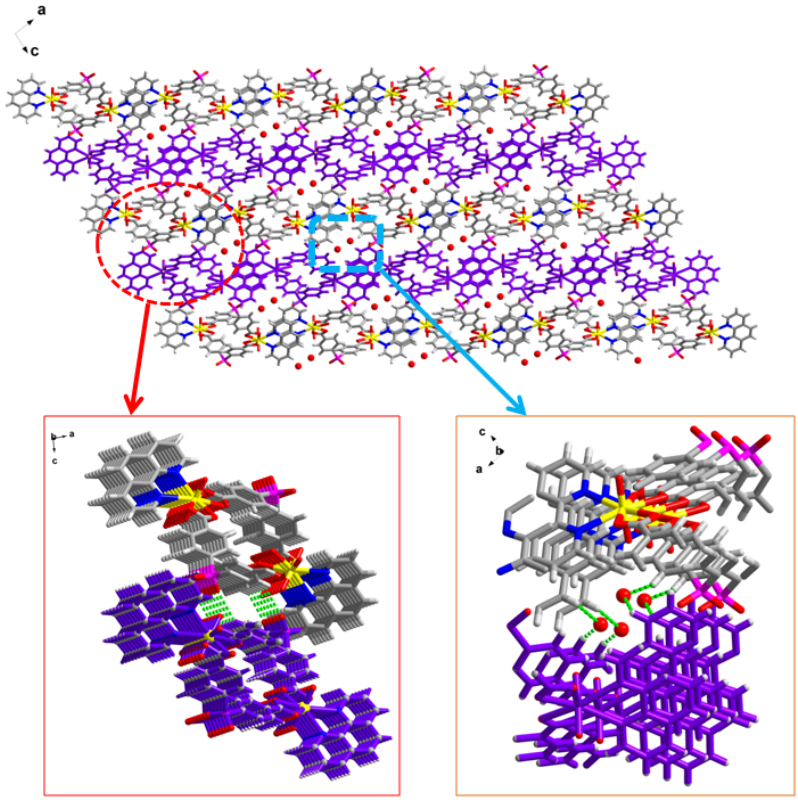

Figure S6. Close packing of compound **2** in three dimeonsions viewed from *b* axis with water molecule located at the cavities (top), weak hydrogen bonds between triple-stranded helices from two adjacent 2D uranyl coordination network (left in the bottom, C(3)-H(3)•••O(8), 2.654(4) Å), and two sets of hydrogen bonds between water molecule and two adjacent sheets (C(13)-H(13)•••O(1W) 2.916(13) Å).

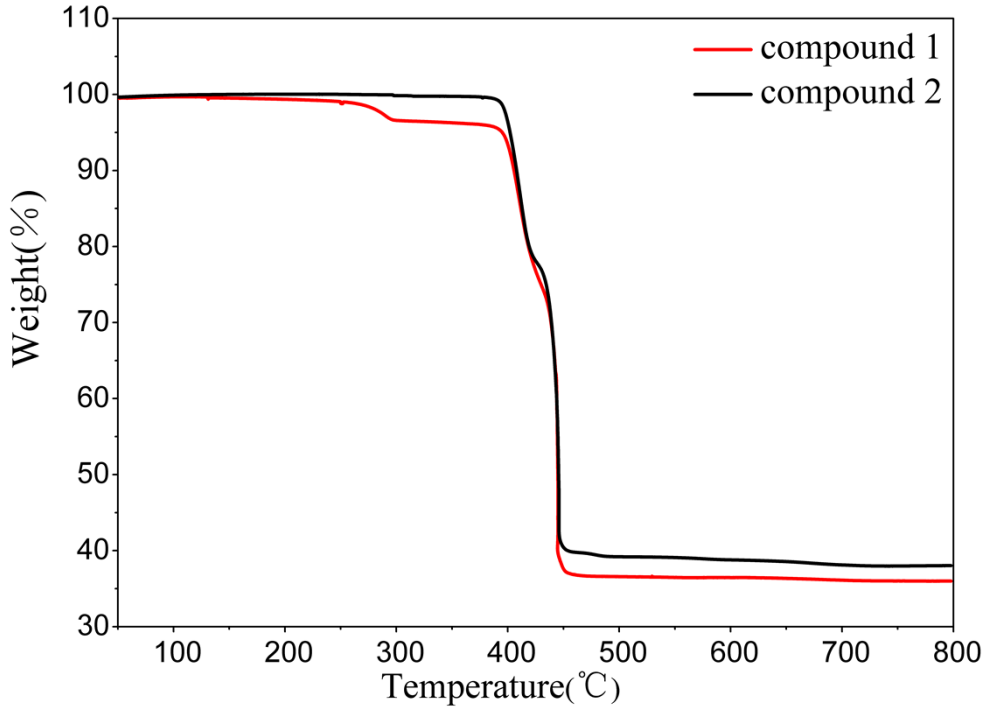

Figure S7. Thermogravimetric analysis for compounds **1** and **2**. Compound **2** with inter-chain π-π stacking interactions displays better thermal stability than the single chain compound **1** with its intra-chain π-π stacking interactions.

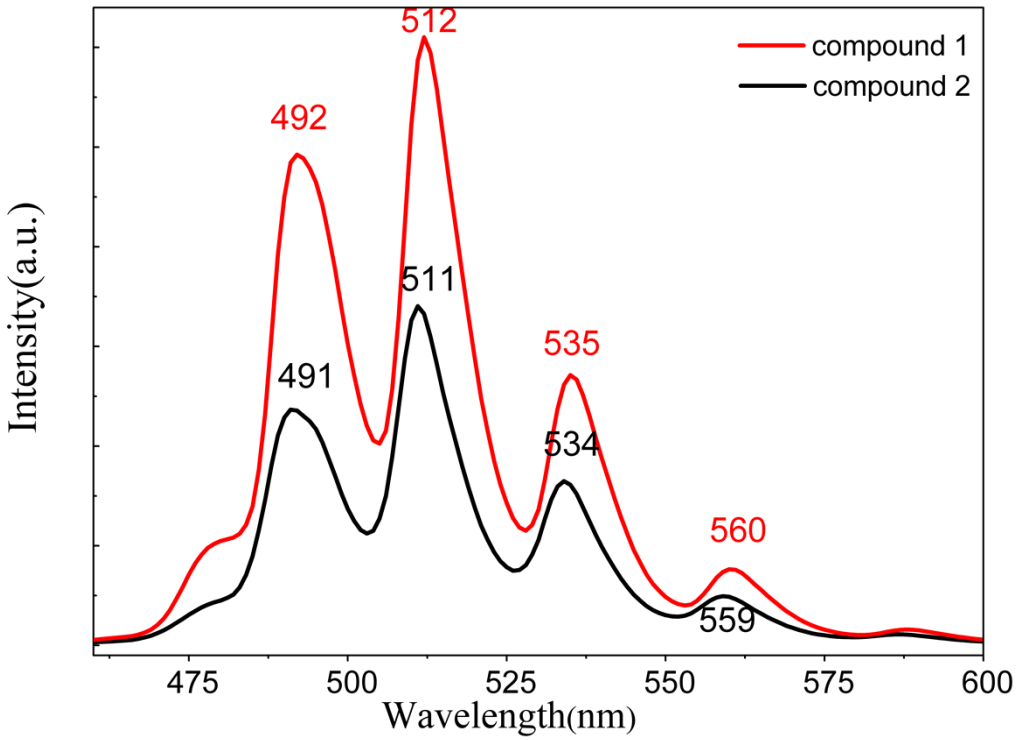

Figure S8. Fluorescence spectra of compound **1** (red color) and compound **2** (black color). Compound **2** with inter-chain π-π stacking interactions displays weaker fluorescent emission than the single chain compound **1** with its intra-chain π-π stacking interactions.

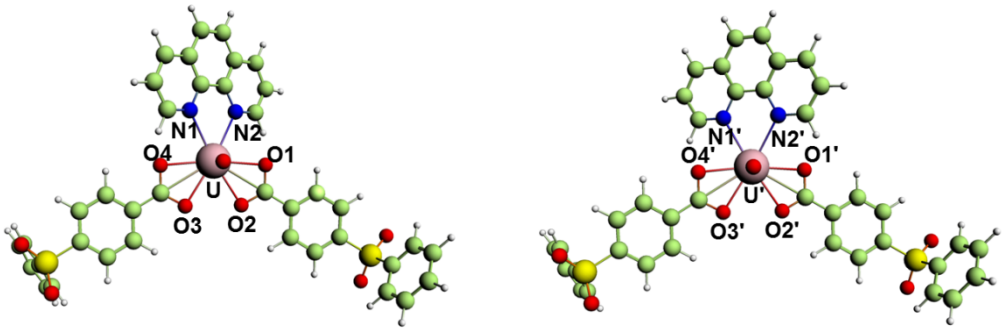

a b

Figure S9. Optimized structures of compounds **1** (a) and **2** (b) by the B3LYP method. White, green, blue, red, yellow, and pink spheres represent H, C, N, O, S, and U, respectively.

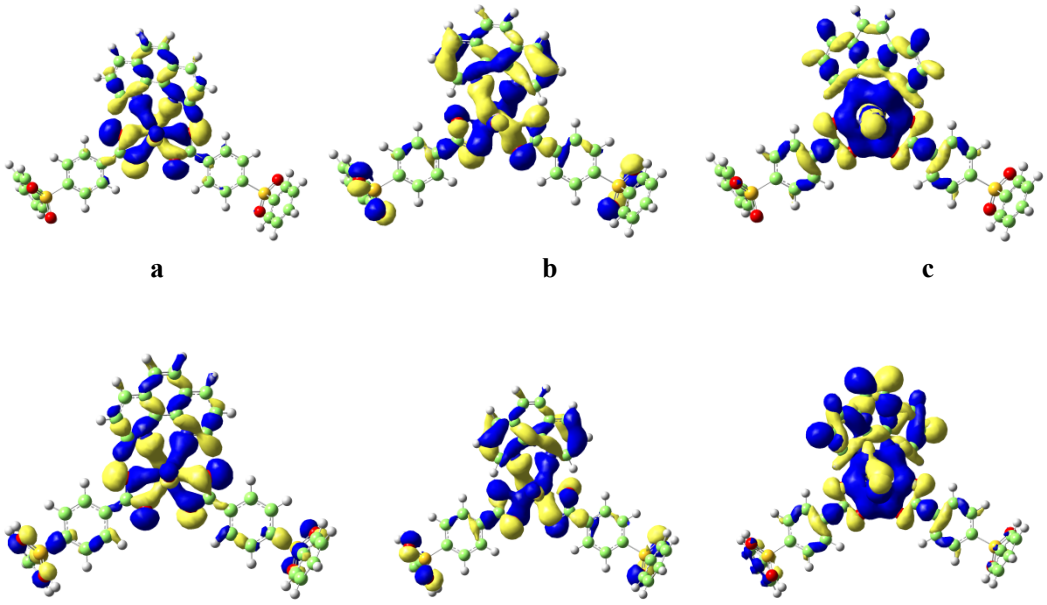

a b c

a' b' c'

Figure S10. The main molecular orbitals (MOs) referring to the U-O and U-N bonding for compounds **1** and **2**.

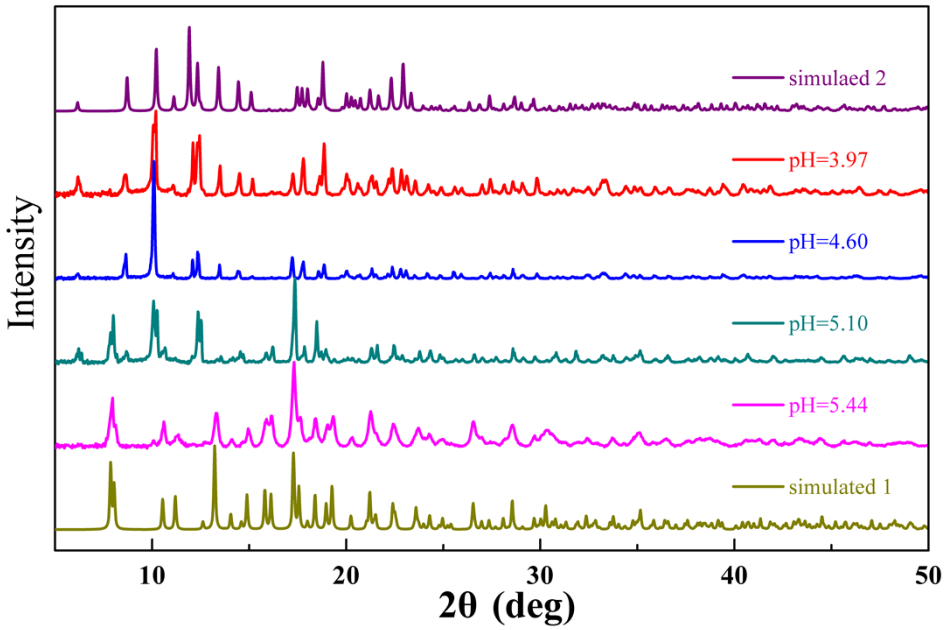

Figure S11. Powder x-ray diffraction (PXRD) patterns demonstrating pH-dependent structural evolution of compounds **1** and **2**. From bottom to top: simulated PXRD of compound **1**; PXRD of solid product at pH=5.44; PXRD of solid product at pH=5.10; PXRD of solid product at pH=4.60; PXRD of solid product at pH=3.97; simulated PXRD of compound **2**.

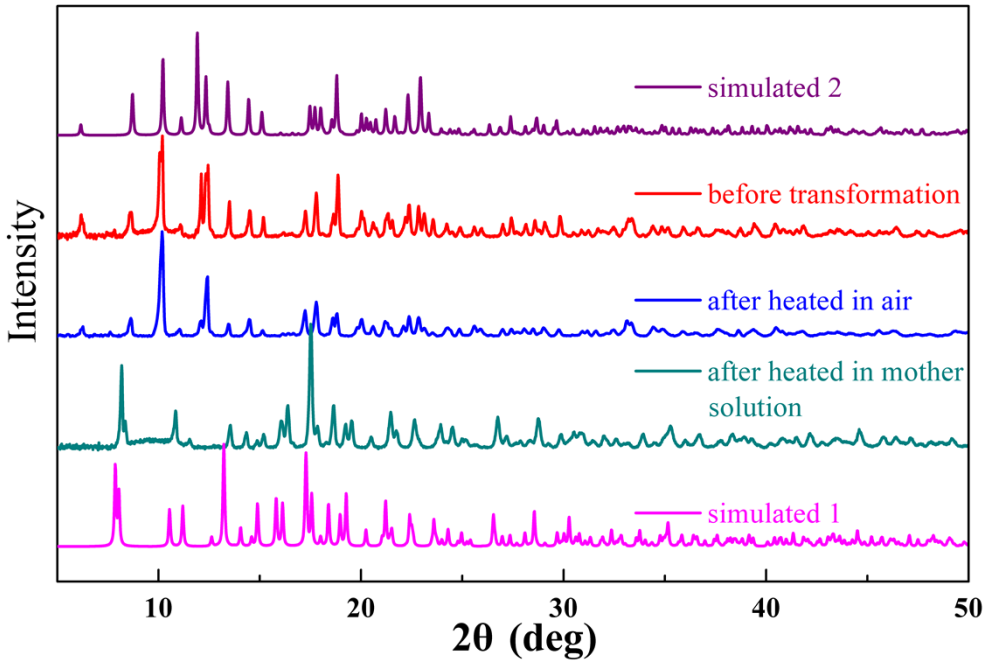

Figure S12. PXRD results before and after the transformation of compound **2** to compound **1** with simulated PXRD patterns of compounds **1** and **2** for comparison: the trial of transformation for **2** in the presence of mother solution reveals the obvious change of PXRD patterns, giving characteristic peaks of compound **1**, whereas the attempt of direct transformation from a solid state of compound **2** in the absence of mother solution shows no change of PXRD patterns before and after the transformation.

Table S1. Selected bond distances (Å) related to uranyl centers and distances (Å) for hydrogen bonds and C-H•••π bonds observed in uranyl compounds **1** and **2**.

		1	
U(1)-O(1)	2.473(6)	**C(14)-H(14)···O(2)**	2.532(5)
U(1)-O(2)	2.470(6)	**C(14)-H(14)···O(3)**	2.511(6)
U(1)-O(3)	2.466(6)	**C(18)-H(18)···O(8)**	2.598(6)
U(1)-O(4)	2.451(6)	**C(17)-H(17)···O(8)**	2.712(6)
U(1)-O(5)	1.773(7)	**C(17)-H(17)···O(5)**	2.789(7)
U(1)-O(6)	1.767(7)	**C(16)-H(16)···O(5)**	2.775(6)
U(1)-N(1)	2.639(7)	**C(27)-H(27)···O(6)**	2.538(7)
U(1)-N(2)	2.613(7)		
		2	
U(1)-O(1)	2.457(4)	**U(1)-N(1)**	2.651(6)
U(1)-O(2)	2.445(4)	**U(1)-N(2)**	2.635(6)
U(1)-O(3)	2.486(4)	**C(11)-H(11)···O(2)**	2.716(4)
U(1)-O(4)	2.451(4)	**C(11)-H(11)···O(3)**	2.686(4)
U(1)-O(5)	1.754(5)	**C(3)-H(3)···O(8)**	2.654(4)
U(1)-O(6)	1.765(4)	**C(13)-H(13)···O(1W)**	2.916(13)

Table S2. Comparison of Selected Calculated and Experimental Bond Lengths (Å) of the U-O Bonds, and the May Bond Order (MBO) of the U-O Bonds for Compounds **1** and **2**.

Compound 1		**U-N1**	**U-N2**	**U-O1**	**U-O2**	**U-O3**	**U-O4**
	Expt.	2.639(7)	2.613(7)	2.473(6)	2.470(6)	2.466(6)	2.451(6)
	Calc.	2.679	2.678	2.476	2.478	2.476	2.477
	MBO	0.302	0.302	0.437	0.443	0.444	0.437
Compound 2		**U'-N1'**	**U'-N2'**	**U'-O1'**	**U'-O2'**	**U'-O3'**	**U'-O4'**
	Expt.	2.651(6)	2.635(6)	2.457(4)	2.445(4)	2.486(4)	2.450(4)
	Calc.	2.677	2.680	2.476	2.478	2.477	2.477
	MBO	0.303	0.303	0.437	0.444	0.444	0.437

Table S3. Percent Contribution of the U-O and U-N Bonding in Compounds **1** and **2**.

Species	MO Orbital	Contributions of Each Atomic Orbital (%)								
		U			O1	O2	O3	O4	N1	N2
		5f	*6d*	*7s*	*2p*	*2p*	*2p*	*2p*	*2p*	*2p*
Compound 1	**a**	10			19	11	10	18	5	5
	b	3	3		4	12	12	5	5	5
	c		1	4	10	7	7	10	5	5
Compound 2	**a'**	9			13	7	9	15	6	6
	b'	3	3		6	12	12	5	5	6
	c'		1	4	10	7	7	10	5	5